PROCESSING OF EXPERIMENTAL SEISMIC ARRAY DATA USING 2-D WIDEBAND INTERPOLATED ROOT-MUSIC

Dmitri V. Sidorovich *Alex B. Gershman* *Johann F. Böhme*

Signal Theory Group, Department of Electrical Engineering
Ruhr University, D-44780 Bochum, Germany
gsh@sth.ruhr-uni-bochum.de

ABSTRACT

2-D elementspace and beamspace extensions of Friedlander's wideband interpolated root-MUSIC technique are applied to azimuth-velocity source location using real seismic data from the GERESS array (Germany). We demonstrate that 2-D interpolated root-MUSIC is able to estimate the parameters of a typical seismic source with a good accuracy. The use of interpolated root-MUSIC and its beamspace modification is motivated by the significant reduction of processing time allowing on-line implementation.

1. INTRODUCTION

Root eigenstructure techniques [1] are known to have much easier 1-D implementations than spectral techniques. Unfortunately, root estimators cannot be applied straightforwardly to non-uniform arrays. To overcome this problem, Friedlander developed an elegant approach [2] based on the idea to interpolate a virtual Uniform Linear Array (ULA) (whose sensor locations are chosen by the user) using the original non-uniform array. It was shown in [3] that in a wideband case, the interpolated array approach can be exploited in a framework of Coherent Signal Subspace (CSS) processing pioneered by Wang and Kaveh [4]. The central idea of [3] is to generate a different virtual ULA for each relevant frequency ω, with the interelement spacing proportional to $1/\omega$ [5]. After this procedure, a collection of virtual ULA's "tuned" to different frequencies is available [3]. The next steps are identical to that of CSS processing [4], [5], i.e., they contain the coherent average of interpolated covariance matrices and application of narrowband root-MUSIC to coherently averaged covariance matrix.

Below, we describe a practical application of the interpolated array approach. We develop simple 2-D elementspace and beamspace extensions of wideband interpolated root-MUSIC using two ULA sets for joint azimuth-velocity estimation. These techniques are then exploited for seismic source localization using experimental data from regional GERESS array located in Bavarian Forest, Germany.

Our research is motivated by the very significant reduction of computational cost of real data processing, which can be achieved using root and beamspace eigenstructure estimators, as compared with computationally expensive wideband ML technique [6]. Additional motivation is a rapidly growing interest of specialists to real data applications of today array processing methods. Our work seems to be the first attempt to apply the interpolated array approach to real data.

This work was supported in parts by international projects of DFG (Germany), GIF (Germany/Israel) and INTAS (Belgium).

2. WIDEBAND SIGNAL MODEL

Assume that an array of p sensors receives wideband signals from q far-field sources. 2-D array will be assumed, because the vertical aperture of the GERESS array is negligible small compared to the horizontal apertures and can be ignored when estimating seismic source parameters [6].

Let the $p \times 1$ array output vector $\boldsymbol{x}(t)$ is observed T seconds which are sectioned into N (possibly overlapping) subintervals of duration T_0. For each subinterval the temporal Fourier transform of the length M is then computed. Let K frequency bins are used. Therefore, the $p \times 1$ Fourier-transformed array vector observations are given by [3]-[5]

$$\boldsymbol{X}(i,\omega_l) = \boldsymbol{A}(\omega_l)\boldsymbol{S}(i,\omega_l) + \boldsymbol{N}(i,\omega_l)\ ,$$
$$i = 1,2,\ldots,N, \quad l = 1,\ldots,K\ , \tag{1}$$

where

$$\boldsymbol{X}(i,\omega_l) = (X_1(i,\omega_l),\ldots,X_p(i,\omega_l))^T\ ,$$
$$\boldsymbol{S}(i,\omega_l) = (S_1(i,\omega_l),\ldots,S_q(i,\omega_l))^T\ ,$$
$$\boldsymbol{N}(i,\omega_l) = (N_1(i,\omega_l),\ldots,N_p(i,\omega_l))^T$$

are the observation, source, and sensor noise vectors, respectively. The steering matrix $\boldsymbol{A}(\omega_l)$ at the frequency ω_l is given by

$$\boldsymbol{A}(\omega_l) = [\boldsymbol{a}(\omega_l,\boldsymbol{\xi}_1),\ldots,\boldsymbol{a}(\omega_l,\boldsymbol{\xi}_q)]\ , \tag{2}$$

where $\boldsymbol{a}(\omega,\boldsymbol{\xi})$ is the steering vector at the frequency ω towards the source with a vector parameter $\boldsymbol{\xi}$. In our case, $\boldsymbol{\xi} = (\xi_x,\xi_y)^T$ is the slowness vector [6]. The model for the steering vector then reads

$$\boldsymbol{a}(\omega_l,\boldsymbol{\xi}) = (e^{-j\omega_l\boldsymbol{\xi}^T\boldsymbol{r}_1},\ldots,e^{-j\omega_l\boldsymbol{\xi}^T\boldsymbol{r}_p})^T\ , \tag{3}$$

where

$$\boldsymbol{\xi} = (\xi_x,\xi_y)^T = \frac{1}{V}(\cos\theta,\sin\theta)^T\ , \tag{4}$$

$\boldsymbol{r}_i = (x_i,y_i)^T$ is the vector coordinate of the ith sensor, whereas θ and V are the source azimuth and wave velocity parameters, respectively. The problem is to estimate the azimuth-velocity pairs $\{\theta_i,V_i\}$ $(i = 1,2,\ldots,q)$.

3. 2-D WIDEBAND INTERPOLATED ROOT-MUSIC

For joint estimation of the source azimuth and wave velocity, a 2-D technique should be applied. In this section, we describe 2-D interpolated wideband root-MUSIC which represents an extension of the 1-D algorithm by Friedlander and Weiss [3] for two sets of

interpolated ULA's. This 2-D algorithm will be used below for processing of the GERESS array dataset. We prefer the root technique to a spectral one (e.g., to 2-D spectral MUSIC) because of evident computational advantages, i.e., much faster implementation avoiding computationally expensive 2-D search over the array manifold.

Let the 2-D array is divided into two n-element (possibly overlapping) subarrays referred hereafter to as subarrays (a) and (b). Similarly to (1), write the $n \times 1$ observation vectors from the first and second subarrays as

$$\boldsymbol{X}_a(i,\omega_l) = \boldsymbol{A}_a(\omega_l)\boldsymbol{S}_a(i,\omega_l) + \boldsymbol{N}_a(i,\omega_l)\ , \qquad (5)$$

$$\boldsymbol{X}_b(i,\omega_l) = \boldsymbol{A}_b(\omega_l)\boldsymbol{S}_b(i,\omega_l) + \boldsymbol{N}_b(i,\omega_l)\ , \qquad (6)$$

respectively. Each subarray is employed for interpolation of the corresponding set of virtual ULA's. Each set contains K virtual ULA's (one ULA per frequency bin) with the interelement spacings $d_{a,c}\omega_c/\omega_l$, and $d_{b,c}\omega_c/\omega_l$, for the sets (a) and (b), respectively. Here $d_{a,c}$ and $d_{b,c}$ are the interelement spacings of the virtual ULA's at the central frequency $\omega_c = 2\pi f_c$. With such choice of virtual ULA's, the virtual array manifold is the same for each frequency. Apparently, this property holds for each set of virtual ULA's. However, the original subarray manifold is different for various frequency bins. Thus, K interpolation matrices [3] have to be exploited for the each set, so that

$$\boldsymbol{B}_{a,l}^H \boldsymbol{a}_a(\omega_l,\boldsymbol{\xi}) = \breve{\boldsymbol{a}}_a(\omega_c,\boldsymbol{\xi})\ , \qquad (7)$$

$$\boldsymbol{B}_{b,l}^H \boldsymbol{a}_b(\omega_l,\boldsymbol{\xi}) = \breve{\boldsymbol{a}}_b(\omega_c,\boldsymbol{\xi})\ , \quad \boldsymbol{\xi} \in \boldsymbol{\Xi}\ , \qquad (8)$$

where $\boldsymbol{B}_{a,l}$ and $\boldsymbol{B}_{b,l}$ are the interpolation matrices designed at the frequency ω_l for the sets (a) and (b), respectively. Here, $\boldsymbol{a}_a(\omega_l,\boldsymbol{\xi})$ is the steering vector of the original subarray (a) at the frequency ω_l, and $\boldsymbol{a}_b(\omega_l,\boldsymbol{\xi})$ is the similar steering vector but for the original subarray (b). The steering vectors $\breve{\boldsymbol{a}}_a(\omega_c,\boldsymbol{\xi})$ and $\breve{\boldsymbol{a}}_b(\omega_c,\boldsymbol{\xi})$ describe the manifold of the virtual ULA's (a) and (b), respectively, at the central frequency ω_c, and $\boldsymbol{\Xi}$ denotes the 2-D interpolation sector.

Since all virtual arrays within the same set have the same manifold, the observations can be combined [3] over K frequency bins in the so-called coherently averaged covariance matrices for the subarrays (a) and (b):

$$\tilde{\boldsymbol{R}}_a = \frac{1}{K}\sum_{l=1}^{K} \boldsymbol{B}_{a,l}^H \hat{\boldsymbol{R}}_a(\omega_l)\boldsymbol{B}_{a,l}\ , \qquad (9)$$

$$\tilde{\boldsymbol{R}}_b = \frac{1}{K}\sum_{l=1}^{K} \boldsymbol{B}_{b,l}^H \hat{\boldsymbol{R}}_b(\omega_l)\boldsymbol{B}_{b,l}\ , \qquad (10)$$

where

$$\hat{\boldsymbol{R}}_a(\omega_l) = \frac{1}{N}\sum_{i=1}^{N} \boldsymbol{X}_a(i,\omega_l)\boldsymbol{X}_a(i,\omega_l)^H\ , \qquad (11)$$

$$\hat{\boldsymbol{R}}_b(\omega_l) = \frac{1}{N}\sum_{i=1}^{N} \boldsymbol{X}_b(i,\omega_l)\boldsymbol{X}_b(i,\omega_l)^H \qquad (12)$$

are the sample covariance matrices at the frequency ω_l for the original subarrays (a) and (b), respectively.

Using the analogy with the 1-D algorithm [3], 2-D wideband interpolated root-MUSIC can be summarized as follows:

Step 1: Obtain the estimates $\tilde{\boldsymbol{R}}_a$ and $\tilde{\boldsymbol{R}}_b$ for the subarrays (a) and (b) (Eqns. (9)-(12)).

Step 2: Assuming spatially white noise at each frequency, obtain the estimates of the noise covariance matrices $\boldsymbol{Q}_a$ and $\boldsymbol{Q}_b$ for subarrays (a) and (b) after the coherent processing as

$$\hat{\boldsymbol{Q}}_a = \frac{\hat{\sigma}^2(\omega_l)}{K}\sum_{l=1}^{K} \boldsymbol{B}_{a,l}^H \boldsymbol{B}_{a,l}\ , \qquad (13)$$

$$\hat{\boldsymbol{Q}}_b = \frac{\hat{\sigma}^2(\omega_l)}{K}\sum_{l=1}^{K} \boldsymbol{B}_{b,l}^H \boldsymbol{B}_{b,l}\ , \qquad (14)$$

where $\hat{\sigma}^2(\omega_l)$ is the estimate of the noise variance at the frequency ω_l.

Step 3: Prewhiten the sensor noise in the matrices $\tilde{\boldsymbol{R}}_a$ and $\tilde{\boldsymbol{R}}_b$ as follows:

$$\overline{\boldsymbol{R}}_a = \hat{\boldsymbol{Q}}_a^{-1/2}\tilde{\boldsymbol{R}}_a\hat{\boldsymbol{Q}}_a^{-1/2}\ , \qquad (15)$$

$$\overline{\boldsymbol{R}}_b = \hat{\boldsymbol{Q}}_b^{-1/2}\tilde{\boldsymbol{R}}_b\hat{\boldsymbol{Q}}_b^{-1/2}\ . \qquad (16)$$

Step 4: Obtain eigendecompositions of the matrices $\overline{\boldsymbol{R}}_a$ and $\overline{\boldsymbol{R}}_b$:

$$\overline{\boldsymbol{R}}_a = \boldsymbol{U}_N\boldsymbol{\Lambda}_N\boldsymbol{U}_N^H + \boldsymbol{U}_S\boldsymbol{\Lambda}_S\boldsymbol{U}_S^H\ , \qquad (17)$$

$$\overline{\boldsymbol{R}}_b = \boldsymbol{V}_N\boldsymbol{\Gamma}_N\boldsymbol{V}_N^H + \boldsymbol{V}_S\boldsymbol{\Gamma}_S\boldsymbol{V}_S^H\ , \qquad (18)$$

where the matrices $\boldsymbol{U}_S$ and $\boldsymbol{U}_N$ contain the signal and noise subspace eigenvectors of $\overline{\boldsymbol{R}}_a$, whereas the diagonal matrices $\boldsymbol{\Lambda}_S$ and $\boldsymbol{\Lambda}_N$ contain its signal and noise subspace eigenvalues. Similarly, the matrices $\boldsymbol{V}_S$ and $\boldsymbol{V}_N$ contain the signal and noise subspace eigenvectors of $\overline{\boldsymbol{R}}_b$, whereas the diagonal matrices $\boldsymbol{\Gamma}_S$ and $\boldsymbol{\Gamma}_N$ contain its signal and noise subspace eigenvalues.

Step 5: Inside the unit circle, find the q closest to the unit circle roots $\{z_{a,1},\ldots,z_{a,q}\}$ and $\{z_{b,1},\ldots,z_{b,q}\}$ of the polynomials

$$D_a(z) = \breve{\boldsymbol{a}}^T(1/z)\hat{\boldsymbol{Q}}_a^{-1/2}\boldsymbol{U}_N\boldsymbol{U}_N^H\hat{\boldsymbol{Q}}_a^{-1/2}\breve{\boldsymbol{a}}(z)\ , \qquad (19)$$

$$D_b(z) = \breve{\boldsymbol{a}}^T(1/z)\hat{\boldsymbol{Q}}_b^{-1/2}\boldsymbol{V}_N\boldsymbol{V}_N^H\hat{\boldsymbol{Q}}_b^{-1/2}\breve{\boldsymbol{a}}(z)\ , \qquad (20)$$

respectively. Here

$$\breve{\boldsymbol{a}}(z) = (1, z^{-1}, \ldots, z^{-(n-1)})^T\ . \qquad (21)$$

Step 6: Find the solutions of the linear system:

$$\boldsymbol{D}\boldsymbol{\xi} = \boldsymbol{f} \qquad (22)$$

for all i and k ($i = 1,\ldots,q$; $k = 1,\ldots,q$), where

$$\boldsymbol{f} = \left(\arg\frac{z_{a,i}}{\omega_c}, \arg\frac{z_{b,k}}{\omega_c}\right)^T\ , \qquad (23)$$

and

$$\boldsymbol{D} = \begin{pmatrix} \Delta x_a & \Delta y_a \\ \Delta x_b & \Delta y_b \end{pmatrix}\ . \qquad (24)$$

Here Δx_a, Δy_a, and Δx_b, Δy_b are the sensor spacings in the virtual arrays (a) and (b), corresponding to the central frequency ω_c.

Step 7: Obtain q pairs of the estimated parameters in a following manner. From q^2 possible solutions of (22), take only q solutions corresponding to the maximal values of the 2-D spectral MUSIC function. This function should be computed using the coherently averaged covariance matrix of the whole 2-D array. When evaluating the 2-D MUSIC function, we do not need to search over the whole array manifold, because only q^2 values of this function

have to be computed. As a result of this step, we obtain the estimates of the slowness vector for each source $\boldsymbol{\xi}_i = (\xi_{x,i}, \xi_{y,i})^T$ $(i = 1, \ldots, q)$.

Step 8: Obtain the azimuth and wave velocity estimates as

$$\theta_i = \arctan(\xi_{y,i}/\xi_{x,i}) \,,$$

$$V_i = \frac{1}{\sqrt{\xi_{x,i}^2 + \xi_{y,i}^2}} \,, \quad i = 1, \ldots, q \,. \tag{25}$$

4. BEAMSPACE EXTENSION

2-D wideband interpolated root-MUSIC can be easily extended onto the beamspace domain. The $m \times m$ $(m < n)$ coherently averaged beamspace covariance matrices

$$\overline{\boldsymbol{R}}_{\mathrm{BS},a} = \boldsymbol{T}_a^H \overline{\boldsymbol{R}}_a \boldsymbol{T}_a \,, \tag{26}$$

$$\overline{\boldsymbol{R}}_{\mathrm{BS},b} = \boldsymbol{T}_b^H \overline{\boldsymbol{R}}_b \boldsymbol{T}_b \tag{27}$$

should be used instead of the $n \times n$ matrices (15) and (16). Here, $\boldsymbol{T}_a$ and $\boldsymbol{T}_b$ are the $n \times m$ beamspace transformation matrices for the virtual ULA's (a) and (b), respectively. These matrices have to be designed at the central frequency ω_c and should correspond to the steering vector model which takes into account noise prewhitening. The beamspace polynomials

$$D_{\mathrm{BS},a}(z) = \breve{\boldsymbol{a}}^T(1/z)\hat{\boldsymbol{Q}}_a^{-1/2}\boldsymbol{T}_a\boldsymbol{U}_N\boldsymbol{U}_N^H\boldsymbol{T}_a^H\hat{\boldsymbol{Q}}_a^{-1/2}\breve{\boldsymbol{a}}(z) \,, \tag{28}$$

$$D_{\mathrm{BS},b}(z) = \breve{\boldsymbol{a}}^T(1/z)\hat{\boldsymbol{Q}}_b^{-1/2}\boldsymbol{T}_b\boldsymbol{V}_N\boldsymbol{V}_N^H\boldsymbol{T}_b^H\hat{\boldsymbol{Q}}_b^{-1/2}\breve{\boldsymbol{a}}(z) \tag{29}$$

should be used instead of (19) and (20) in **Step 5**. Note that unlike (19) and (20), the matrices $\boldsymbol{U}_N$ and $\boldsymbol{V}_N$ in (28) and (29) should be constructed from the noise subspace eigenvectors of the beamspace coherently averaged covariance matrices $\overline{\boldsymbol{R}}_{\mathrm{BS},a}$ and $\overline{\boldsymbol{R}}_{\mathrm{BS},b}$, respectively.

5. EXPERIMENTAL SEISMIC DATA PROCESSING

The configuration of the GERESS array in the horizontal plane is shown in Fig. 1. In order to provide a reasonable quality of array interpolation and to avoid spatial aliasing phenomena, only a part of array sensors was involved in the processing. These sensors are shown in black color in Fig. 1. Remaining sensors are shown in white color. It follows from Fig. 1 that the partially overlapped original subarrays (a) and (b) were used.

The 120 s data record of the regional seismic event caused by an iron mine explosion on the distance of 171 km was selected for analysis. Note that the same data record was analysed in [6] using the wideband ML technique. We use this data batch in order to allow a comparison of our results with the results of [6]. As in [6], the sliding window with the length $T_0 = 3.2$ s was used, with $M = 128$ sampling values (this corresponds to the sampling frequency 40 Hz). The overlap between the neighboring windows was 0.5 s (20 sampling values). In order to increase the number of snapshots N, the Thompson's multiwindow technique with $L = 3$ was exploited. For each frequency bin, $N = L = 3$ was used corresponding to 3 Thompson windows for a single sliding window. Unfortunately, the use of several sliding windows ($N > 3$) was not possible because of a highly non-stationary (transient) behavior of the analysed signal.

Fig. 2 shows the interpolated arrays (a) and (b) corresponding to the central frequency $f_c = 3.125$ Hz. A total of $K = 9$ "well

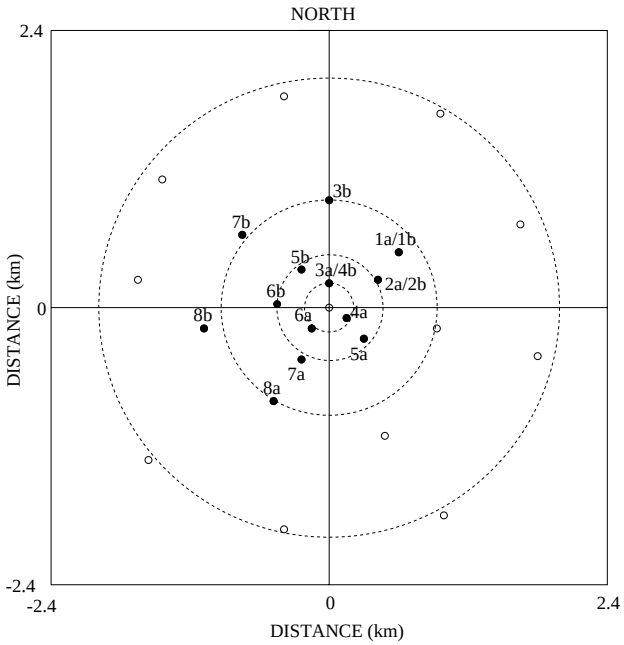

Figure 1: Configuration of GERESS array in the horizontal plane (Bavarian Forest, Germany, 25 sensors). The sensors used for array interpolation (original subarrays (a) and (b)) are shown in the black color. Remaining sensors are shown in the white color.

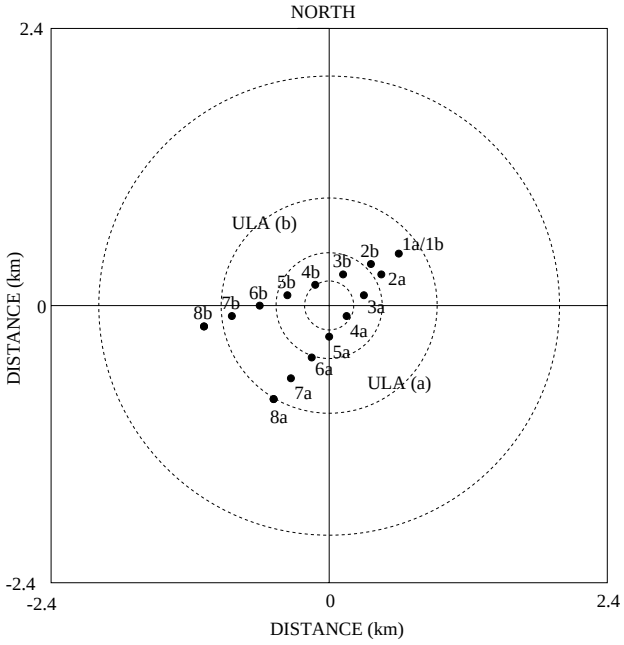

Figure 2: The interpolated (virtual) ULA's (a) and (b) corresponding to the central frequency $f_c = 3.125$ Hz. The virtual ULA's corresponding to other frequency bins are not shown.

separated" frequency bins from the frequency band $[0.625 \ldots 6.25]$ Hz were used. The interpolation sector Ξ taken corresponds to the velocity interval $[3 \ldots 8]$ km/s and the azimuth interval $[100° \ldots 160°]$. The interpolation matrices were designed using the simple least squares fit within the interpolation sector [2].

The results of real data processing are shown in Fig. 3 a-g. For estimating the number of sources, the coherently averaged MDL-detector was employed. Fig. 3 a depicts the analysed signal in the single (reference) sensor. One can observe both P- and S-waves, where the "fast" P-wave arrives prior to the "slow" S-wave [6]. Fig. 3 b,c shows the azimuth and velocity estimates using narrowband elementspace interpolated root-MUSIC. In these subplots, only the single central frequency was used (without coherent averaging over the frequency band). One can observe from these subplots that the variability of the narrowband estimate is unacceptably high. Based on this poor estimate, one can neither distinguish between P- and S waves, nor estimate the azimuth and velocity parameters. Fig. 3 d,e displays the azimuth and velocity estimates using wideband elementspace interpolated root-MUSIC. The coherent processing over the whole frequency band was used. It follows from this part of Fig. 3 that the coherent wideband processing helps to localize the azimuth of the source and to distinguish clearly between the fast and slow P- and S-components in the velocity estimate. The wideband estimates of the azimuth and velocity are in excellent agreement with the results of [6]. The last two subplots (Fig. 3 f,g) show the 2-D estimates provided by wideband beamspace interpolated root-MUSIC. Beamspace transformation with the dimension $m = 3$ was exploited. The same sector Ξ was employed both for the design of beamspace transformation and interpolation matrices. Beamspace matrices were designed using spheroidal sequences approach. The beamspace velocity estimates seem to be even slightly better than that depicted in Fig. 3 d,e, because they tend to be more stable. Again, P- and S-waves corresponding to different velocities can be clearly found in the plot.

Comparing our results with the results of [6], we can claim that the accuracy of 2-D wideband interpolated root-MUSIC is slightly worse as compared to that of the wideband ML method. However, the processing cost of interpolated root-MUSIC is dramatically lower than that of the ML technique, especially when the beamspace processing is used. In particular, the comparison of typical processing times and sampling rates shows that the ML technique can be used only for off-line processing, whereas interpolated root-MUSIC can be exploited for on-line implementation.

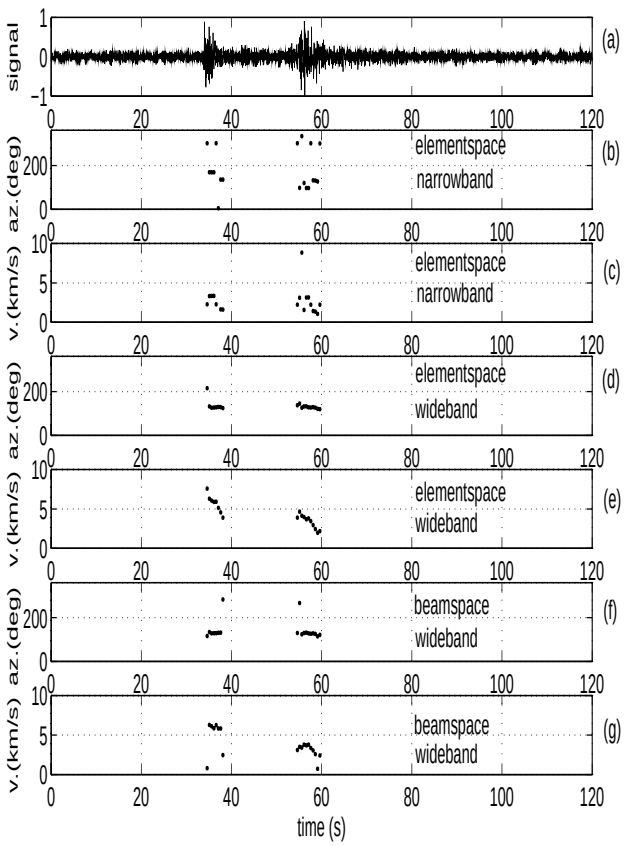

Figure 3: Results of real data processing. a). Analysed signal in the single reference sensor, b). Source azimuth estimate via narrowband elementspace interpolated root-MUSIC, c). Wave velocity estimate via narrowband elementspace interpolated root-MUSIC, d). Source azimuth estimate via wideband elementspace interpolated root-MUSIC, e). Wave velocity estimate via wideband elementspace interpolated root-MUSIC, f). Source azimuth estimate via wideband beamspace interpolated root-MUSIC, g). Wave velocity estimate via wideband beamspace interpolated root-MUSIC.

6. CONCLUSIONS

In this paper, the 2-D elementspace and beamspace extensions of Friedlander's wideband interpolated root-MUSIC estimator have been developed. The estimators considered exploit two sets of interpolated ULA's for joint azimuth-velocity estimation. We have applied these techniques to experimental seismic data analysis using GERESS array dataset. The results of processing of a typical regional seismic event have demonstrated that a very good estimation accuracy can be achieved.

7. REFERENCES

[1] A.J. Barabell, "Improving the resolution performance of eigenstructure-based direction-finding algorithms," in *Proc. ICASSP'83*, Boston, MA, pp. 336-339, May 1983.

[2] B. Friedlander, "The interpolated root-MUSIC algorithm for direction finding," *Signal Processing*, vol. 30, pp. 15-25, 1993.

[3] B. Friedlander and A.J. Weiss, "Direction finding for wideband signals using an interpolated array," *IEEE Trans. Signal Processing*, vol. SP-41, pp. 1618-1634, Apr. 1993.

[4] H. Wang and M. Kaveh, "Coherent signal-subspace processing for the detection and estimation of angles of arrival of multiple wide-band sources," *IEEE Trans. Acoust., Speech, Signal Processing*, vol. ASSP-33, pp. 823-831, Aug. 1985.

[5] J. Krolik and D. Swingler, "Focused wide-band array processing via spatial resampling," *IEEE Trans. Acoust., Speech, Signal Processing*, vol. ASSP-38, pp. 356-360, Feb. 1990.

[6] D.V. Sidorovich, C.F. Mecklenbräuker, and J.F. Böhme, "Sequential test and parameter estimation for array processing of seismic data," *Proc. 8th IEEE Workshop on Stat. Sign. Array Processing*, Corfu, Greece, pp. 256-259, June 1996.